Quantum magnetic properties of the $SU(2N)$ Hubbard model in the square lattice: A quantum Monte Carlo study

Zi Cai,[1,2] Hsiang-Hsuan Hung,[1,3] Lei Wang,[4] and Congjun Wu[1]

[1]*Department of Physics, University of California, San Diego, California 92093, USA*
[2]*Department of Physics and Arnold Sommerfeld Center for Theoretical Physics, Ludwig-Maximilians-Universität München, Theresienstr. 37, 80333 Munich, Germany*
[3]*Department of Electrical and Computer Engineering, University of Illinois, Urbana, Illinois 61801, USA*
[4]*Theoretische Physik, ETH Zurich, 8093 Zurich, Switzerland*

We employ the determinant projector quantum Monte Carlo method to investigate the ground-state magnetic properties in the Mott insulating states of the half-filled $SU(4)$ and $SU(6)$ Fermi-Hubbard model in the two-dimensional square lattice, which is free of the sign problem. The long-range antiferromagnetic Neel order is found for the $SU(4)$ case with a small residual Neel moment. Quantum fluctuations are even stronger in the $SU(6)$ case. Numeric results are consistent with either a vanishing or even weaker Neel ordering than that of $SU(4)$.

I. INTRODUCTION

Quantum antiferromagnetism (AF) has been an important topic of the two-dimensional (2D) strongly correlated systems for decades. For the Hubbard model in the 2D square lattice, the charge gap opens starting from an infinitesimal U. The low-energy physics is described by the AF Heisenberg model. For the $SU(2)$ case, quantum spin fluctuations are not strong enough to suppress the AF long-range order.[1,2] Augmenting the symmetry to $SU(N)$ or $Sp(2N)$ enhances quantum spin fluctuations,[3–5] which can be handled by the systematic $1/N$-analysis. The $SU(N)$ spin operators can be formulated in terms of either bosonic or fermionic representations. The bosonic large-N analysis finds gapped quantum paramagnetic states exhibiting various crystalline orderings,[6] while the fermionic one gives rise to gapless flux-type spin liquid states.[4,7] However, its stability remains an open issue. On the other hand, short-range resonating-valence-bond-type gapped spin liquid states have also been extensively studied.[8–10]

Due to the difficulty of handling strong correlations, numerical simulations have been playing an important role in the study of exotic quantum spin states.[11–22] Whether the spin-disordered quantum insulating states exist in the honeycomb lattice or not is currently under debate.[15,23] A constrained path-integral quantum Monte Carlo (QMC) simulation finds evidence of a gapless spin disordered phase in the square lattice with π flux per plaquette.[16] Evidence of gapped spin liquid phases has also been found by the density-matrix-renormalization-group simulations of the frustrated Heisenberg models in the Kagome lattice[17,24] and in the square lattice with diagonal couplings.[18]

The Fermi-Hubbard models with $2N$ components possessing the $SU(2N)$ or $Sp(2N)$ symmetries are not only of academic interest now, but also have become the goal of experimental efforts in ultracold atom physics.[25] It was first proposed to use large-spin alkali and alkaline-earth atoms to realize the $Sp(2N)$ and $SU(2N)$ Hubbard models in Ref. 26,27 for the special case of $2N = 4$ with the proof of a generic $Sp(4)$ symmetry without fine tuning. Currently, the $SU(6)$ and $SU(10)$ symmetric systems of ^{173}Yb and ^{87}Sr atoms have been

realized, respectively.[28–31] In particular, the ^{173}Yb atoms have been loaded into optical lattices to realize the $SU(6)$ Hubbard model, and the charge excitation gap has been observed.[29,31] It has also been expected that Pomeranchuk cooling is efficient in the large-N case to further cool the system down to the temperature scale of the AF exchanges.[32–34]

In this paper, we investigate the magnetic properties of the half-filled $SU(2N)$ Hubbard models with $2N = 4$ and 6 by the sign-problem free determinant projector quantum Monte Carlo (QMC) method. For the $SU(4)$ case, the ground state remains AF ordered as in the case of $SU(2)$ although the residual spin moments are much weaker. For the $SU(6)$ case, we find that the residual Neel moments are either absent or extremely small beyond the resolution limit of our simulations on structure factors and the finite-size scaling scheme.

The rest of the paper is organized as follows. We define the $SU(2N)$ Hubbard model in Sec. II, and present parameters for QMC simulations in Sec. III. The simulation results of magnetic properties for the $SU(4)$ and $SU(6)$ cases are presented in Sec. IV and Sec. V, respectively. The single-particle gaps are shown in Sec. VI. Conclusions are made in Sec. VII.

II. $SU(2N)$ HUBBARD MODEL

In this section, we define the $SU(2N)$ Hubbard model, related operators, and correlation functions. The $SU(2N)$ Fermi Hubbard model in the 2D square lattice at half-filling is defined as

$$H = -t \sum_{\langle i,j \rangle, \alpha} \{c_{i\alpha}^\dagger c_{j\alpha} + \text{H.c.}\} + \frac{U}{2} \sum_i (n_i - N)^2, \quad (1)$$

where t is scaled as 1 below; α represents spin indices running from 1 to $2N$; $\langle i,j \rangle$ denotes the summation over the nearest neighbors; n_i is the particle number operator on site i defined as $n_i = \sum_{\alpha=1}^{2N} c_{i\alpha}^\dagger c_{i\alpha}$. Equation (1) is invariant under the particle-hole transformation in bipartite lattices as $c_{i\alpha} \rightarrow (-)^i c_{i\alpha}^\dagger$, and thus the average filling per site $\langle n_i \rangle = N$. Similarly to the case of $SU(2)$, the $SU(2N)$ Hubbard model at half-filling in

bipartite lattices is free of the sign problem for an arbitrary value of $2N$.

Let us fix the convention of the $SU(2N)$ generators. The Hilbert space on site i filled with $r(1 \leqslant r \leqslant 2N)$ fermions forms the $SU(2N)$ representation described by the single-column Young pattern denoted as 1^r where r is the number of rows. For these 1^r representations, the $SU(2N)$ generators are defined as

$$J^{\alpha\beta}(i) = c_{i\alpha}^\dagger c_{i\beta} - \frac{\delta^{\alpha\beta}}{2N}\sum_{\gamma=1}^{2N} c_{i\gamma}^\dagger c_{i\gamma}. \qquad (2)$$

Another standard definition is through the generalized Gell-Mann matrices $c_{i\alpha}^\dagger \lambda_{\alpha\beta}^a c_{i\beta}$ with $1 \leqslant a \leqslant 4N^2 - 1$ and the normalization condition of $\mathrm{tr}[\lambda^a \lambda^b] = \frac{1}{2}\delta^{ab}$. The definition in Eq. (2) has a simple commutation relation as $[J^{\alpha\beta}, J^{\gamma\delta}] = \delta_{\beta\gamma}J^{\alpha\delta} - \delta_{\alpha\delta}J^{\gamma\beta}$. However, the price is that not all of the operators of Eq. (2) are independent, which satisfy the constraint $\sum_\alpha J^{\alpha\alpha} = 0$.

The quadratic Casimir operator is expressed as $C_2(2N) = \frac{1}{2}\sum_{\alpha\beta} J^{\alpha\beta}(i)J^{\beta\alpha}(i)$. For the 1^r representation denoted by the Young pattern with a single column with r boxes, its value is related to the filling number r through the Fierz identity as

$$C_2(2N,r) = r(2N - r)(2N + 1)/(4N). \qquad (3)$$

In the large-U limit in which charge fluctuations are negligible, each site represents the self-conjugate representation 1^N. The two-site equal time spin-spin correlation function is defined as

$$C_{J,SU(2N)}(i,j) = \frac{1}{C_2(2N,N)}\sum_{\alpha,\beta}\frac{1}{2}\langle J^{\alpha\beta}(i)J^{\beta\alpha}(j)\rangle, \qquad (4)$$

where $C_2(2N,N) = N(2N+1)/4$ is the Casimir for 1^N representation. $C_{J,SU(2N)}(i,i)$ approaches 1 in the large-U limit. The normalized spin structure factor at the AF wave vector $\vec{Q}$ is defined as

$$S_{SU(2N)}(\vec{Q}) = \frac{1}{C_2(2N,N)}\sum_{\alpha\beta}\frac{1}{2}\langle J^{\alpha\beta}(\vec{Q})J^{\beta\alpha}(\vec{Q})\rangle, \qquad (5)$$

where $J^{\alpha\beta}(\vec{Q}) = \frac{1}{L}\sum_i e^{i\vec{Q}\cdot\vec{r}_i} J^{\alpha\beta}(i)$. The imaginary-time-displaced spin-spin correlations at wave vector $\vec{Q}$ are defined as

$$S_{SU(2N)}(\vec{Q},\tau) = \sum_{\alpha\beta}\langle J^{\alpha\beta}(\vec{Q},\tau)J^{\beta\alpha}(\vec{Q},0)\rangle, \qquad (6)$$

which are used to extract spin gaps below.

For the usual case of $SU(2)$, i.e., $2N = 2$, the generators of Eq. (2) are reduced to

$$J^{11}(i) = \hat{S}_i^z = \frac{1}{2}(n_{i\uparrow} - n_{i\downarrow}) = -J^{22}(i) \qquad (7)$$

$$J^{12}(i) = \hat{S}_i^+ = c_{i\uparrow}^\dagger c_{i\downarrow} = [J^{21}(i)]^\dagger, \qquad (8)$$

which satisfies the constraint $J^{11}(i) + J^{22}(i) = 0$, and the Casimir for 1^1 representation $C_2(2,1) = 3/4$. The correlation function in Eq. (4) becomes

$$C_{J,SU(2)}(i,j) = \frac{4}{3}\left(\hat{S}_i^x \hat{S}_j^x + \hat{S}_i^y \hat{S}_j^y + \hat{S}_i^z \hat{S}_j^z\right), \qquad (9)$$

where $S_i^{x,y,z}$ are the usual spin-$\frac{1}{2}$ operators.

III. PARAMETERS FOR THE QMC SIMULATIONS

We use the determinant projector QMC method for fermions with the periodic boundary condition as described in Appendix A.[35–37] The simulated system sizes $L \times L$ range from $L = 4$ to 16. Finite-size scaling is performed to extrapolate the ground-state properties in the thermodynamic limit. The initial trial wave function is the ground state of the free part of Eq. (1) to whose hopping integral is attached a small flux to break the degeneracy.[15] Such a Slater-determinant plane-wave state for the imaginary-time evolution is assumed to be nonorthogonal to the true ground state of the entire Hamiltonian. The second-order Suzuki-Trotter decomposition is performed with the imaginary time step $\Delta\tau = 0.05$. The convergence of the simulation results with respect to different values of $\Delta\tau$ has been checked. The length of the imaginary-time evolution is $\beta = 40$. For the $SU(2)$ case, the Hubbard-Stratonovich (HS) transformation is usually performed by using the discrete Ising spin fields.[1] However, the spin channel decomposition does not easily generalize to the $SU(2N)$ case due to the increasing of spin components. Instead, we follow the approximate discrete HS decomposition in the density channel at the price of involving complex numbers.[38] The error of this approximation is at the order $(\Delta\tau)^4$, smaller than that of the Suzuki-Trotter decomposition, thus is negligible. This method has the advantage that the $SU(2N)$ symmetry is maintained explicitly, and also it easily generalizes to large values of $2N$. For the largest lattice size we simulated ($L = 16$), the typical CUP time for a QMC thread with 1000 warmup steps plus 1000 QMC steps is about 50 hours, and 128 QMC threads are taken to evaluated the average values and error bars of the physical quantities of the system.

IV. MAGNETIC PROPERTIES OF THE $SU(4)$ CASE

In this section, we present the study of quantum spin fluctuations starting with the $SU(4)$ case in the square lattice, in which long-range Neel ordering is found.

The finite-size scaling of the spin structure factor $\frac{1}{L^2}S_{SU(4)}(\vec{Q})$ at the AF wave vector $\vec{Q} = (\pi,\pi)$ is plotted in Fig. 1(a). For example, at $U = 8$, it extrapolates to a small but finite value of $s_0 = 0.025$ as $L \to \infty$, which indicates the existence of the AF long-range Neel order. In comparison, for the $SU(2)$ case at the same value of U, the extrapolated value of $\lim_{L\to\infty}\frac{1}{L^2}S_{SU(2)}(\vec{Q}) \approx 0.118$. This shows the enhancement of quantum spin fluctuations as $2N$ increases.

Let us bipartition the lattice into A and B sublattices. One typical classic $SU(4)$ Neel configuration is that A sites are filled with components 1 and 2, and B sites are filled with components 3 and 4. $SU(4)$ is a rank-3 Lie group, and thus its Cartan algebra has three commutable generators defined as $K_{1,2} = \frac{1}{2\sqrt{2}}[(n_1 - n_2) \pm (n_3 - n_4)]$, and $K_3 = \frac{1}{2\sqrt{2}}[(n_1 + n_2) - (n_3 + n_4)]$. Each site of the above $SU(4)$ configuration is a singlet of $K_{1,2}$, and with the eigenvalues of $\pm\frac{1}{\sqrt{2}}$ for K_3. The AF long-range-ordered states possess gapless Goldstone modes, and the Goldstone manifold is the eight-dimensional Grassmann one $U(4)/[U(2) \times U(2)]$. The spin excitations
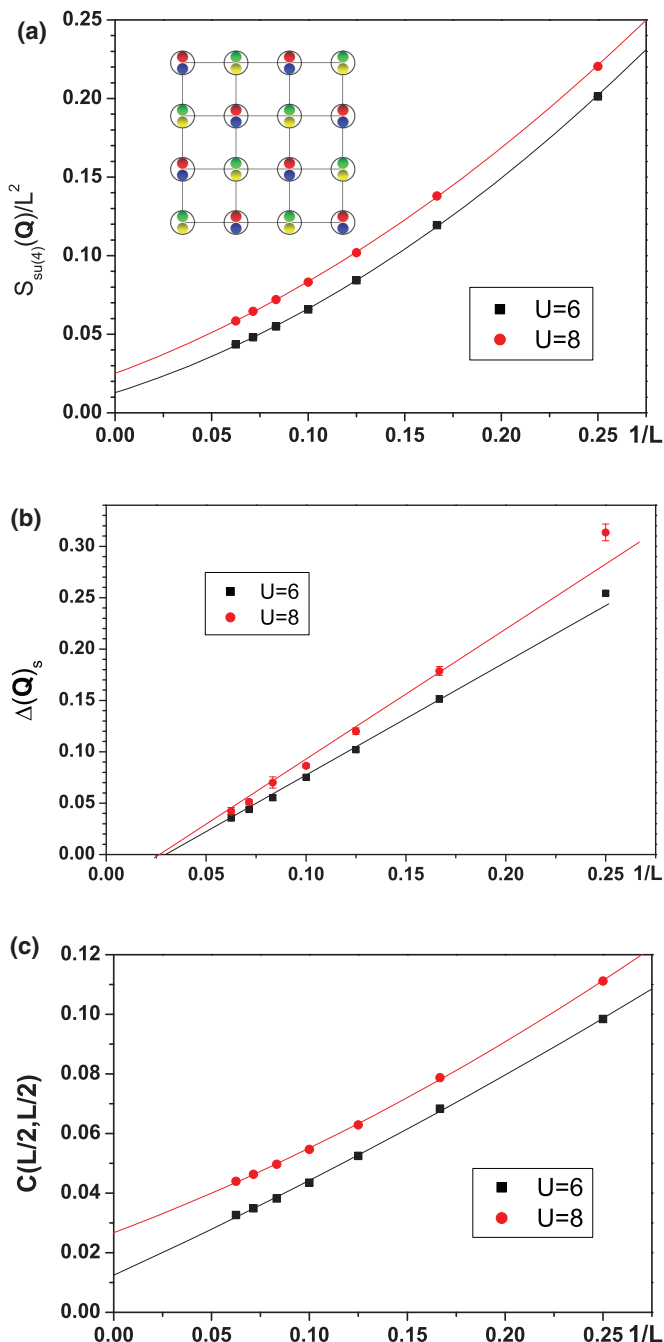
FIG. 1. (Color online) The half-filled $SU(4)$ Hubbard model in the square lattice. (a) The appearance of the AF long-range order from the finite-size scaling of the spin structure factor at $\vec{Q} = (\pi,\pi)$ for $U = 6$ and 8. Solid curves are quadratic fits of data. The inset shows a typical $SU(4)$ AF configuration in which different colors represent different spin components. (b) The absence of the spin gap from the finite-size scaling of $\Delta_s(\vec{Q})$. (c) The scalings of the farthest point correlations $C_{J,SU(4)}(L/2,L/2)$ for $U = 6$ and 8.

from the slope of $\ln S_{SU(4)}(\vec{Q},\tau)$ vs τ. The finite-size scaling is plotted in Fig. 1(b), which shows the absence of spin gap consistent with the long-range AF ordering. To confirm the existence of the AF long-range order in the ground state, we also plotted the farthest two-point equal-time spin-spin correlations $C_{J,SU(4)}(L/2,L/2)$ as a function of L, as shown in Fig. 1(c). The extrapolated values in the thermodynamics
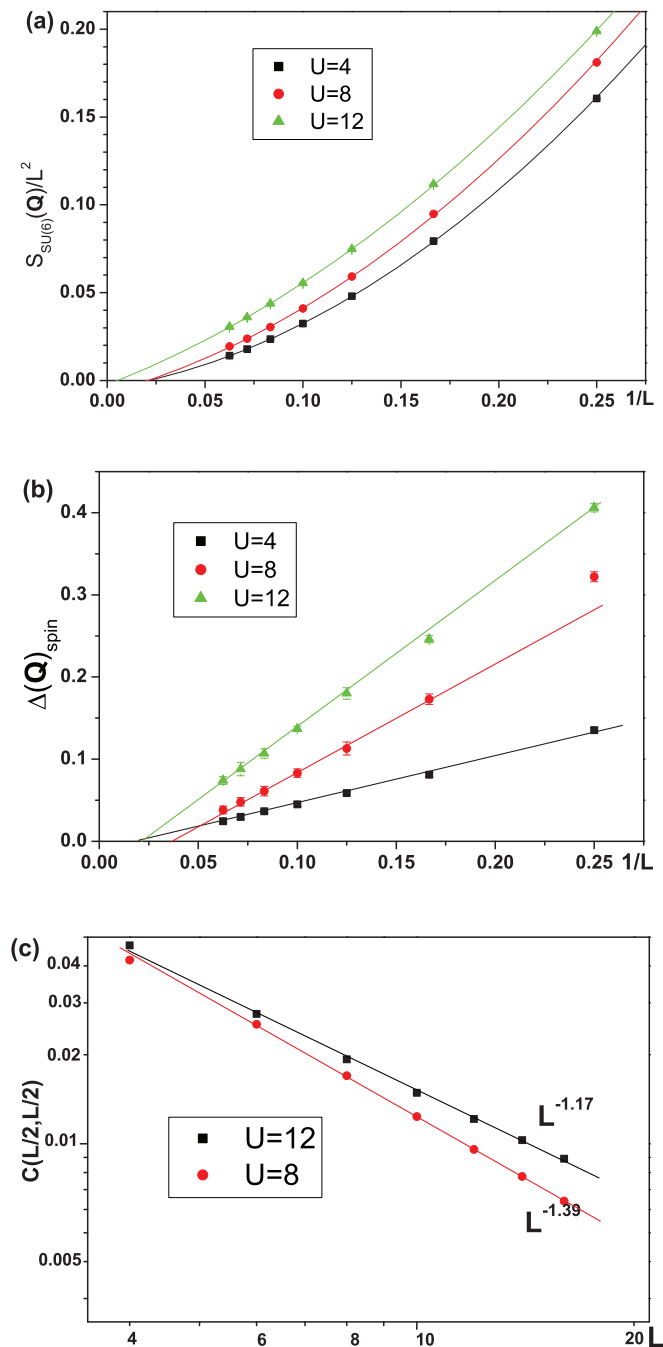

FIG. 2. (Color online) Spin correlations of the half-filled $SU(6)$ Hubbard model. (a) The finite-size scalings of the spin structure factors at $\vec{Q} = (\pi,\pi)$ at $U = 4,8$, and 12 are consistent with either zero or a very weak Neel ordering. Solid curves are quadratic fits. (b) The finite-size scalings $\Delta_s(\mathbf{Q})$ show the absence of spin gap. (c) The scalings of the farthest point correlations $C_{J,SU(6)}(L/2,L/2)$ for $U = 8$ and 12.

carry quantum numbers of $K_{1,2,3}$ as $(\pm\frac{1}{\sqrt{2}},0,\pm\frac{1}{\sqrt{2}})$ and $(0,\pm\frac{1}{\sqrt{2}},\pm\frac{1}{\sqrt{2}})$.

To verify the absence of spin gap, we calculate the imaginary-time-displaced spin correlation function $S_{SU(4)}(\vec{Q},\tau)$.[39,40] The finite-size spin-gap $\Delta_s(\vec{Q},1/L)$ is fitted

limits agree very well with those obtained from the spin structure factors.

V. MAGNETIC PROPERTIES OF THE $SU(6)$ CASE

In this section, we present the QMC simulation results for the $SU(6)$ case in which quantum spin fluctuations become even stronger.

The QMC simulation of the spin structure factors at $\vec{Q} = (\pi,\pi)$ is presented in Fig. 2(a). The finite size scalings of the $SU(6)$ AF structure factor for all the cases of $U = 4, 8$, and 12 extrapolate to zero. However, because the $1/L$ extrapolation of the AF structure factor is proportional to the square of the AF moments, the possibility of a weak AF long-range order cannot be excluded. For example, a Neel moment at the order of 10^{-2} corresponds to the structure factor at the order of 10^{-3} or 10^{-4}, which is beyond our current resolution limit. We further calculate the spin gap value at $\vec{Q} = (\pi,\pi)$ from the imaginary-time-displaced $SU(6)$ spin correlation function $S_{SU(6)}(\vec{Q},\tau)$, and plot the extracted spin gap values in Fig. 2(b). The finite-size scaling shows the vanishing of spin gap in the $SU(6)$ case for all the three values of $U = 4, 8$, and 12. The vanishing of spin gaps is also consistent with very small but nonzero AF moments. The two-point equal-time spin-spin correlations $C_{J,SU(6)}(L/2,L/2)$ are calculated and plotted in Fig. 2(c), which are fitted with algebraic correlations

as $C_{J,SU(6)}(L/2,L/2) \approx L^{-\eta}$. However, due to the limited sample size, these algebraic correlations are well fitted at a intermediate length scale. We still cannot exclude the possibility of small long-range AF moments.

We further check other possible ordering patterns involving two neighboring sites. At half filling, the total particle number on a bond is $2N$, which is sufficient to form a $SU(2N)$ singlet to minimize the spin superexchange energy. We consider ordering patterns in the spin singlet channel with translational symmetry breaking. The bond dimer and current operators are defined as the real and imaginary parts of the hopping amplitudes between nearest neighbors as

$$D_{ij} = \sum_\alpha c_{i,\alpha}^\dagger c_{j,\alpha} + \text{H.c.}, \quad F_{ij} = \sum_\alpha i(c_{i,\alpha}^\dagger c_{j,\alpha} - \text{H.c.}),$$

(10)

and d-density-wave (DDW) operators as $DDW(i) = (-)^i \sum_j F(i,j)$ where $\vec{r}_j - \vec{r}_i = \pm\hat{e}_x$, and $\pm\hat{e}_y$. In the large U limit, the Heisenberg term $S^{\alpha\beta}(i)S^{\beta\alpha}(j)$ is generated from the second-order virtual hopping process, thus D_{ij} can be used
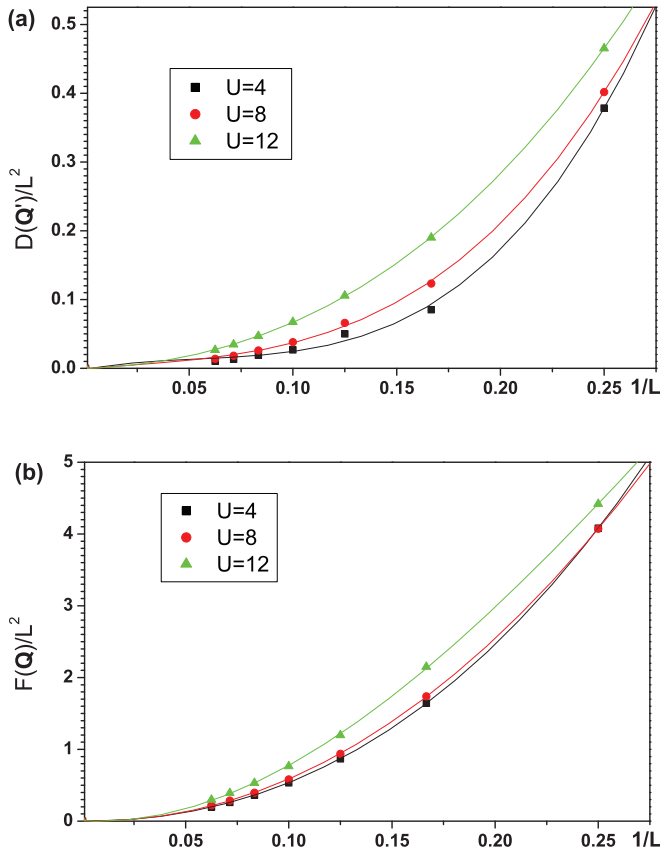

FIG. 3. (Color online) Spin singlet channel operators of the half-filled $SU(6)$ Hubbard model. (a) The finite-size scaling of the columnar dimer structure factors at $\vec{Q}' = (\pi,0)$. (b) The finite-size scaling of the DDW structure factors at $\vec{Q} = (\pi,\pi)$.
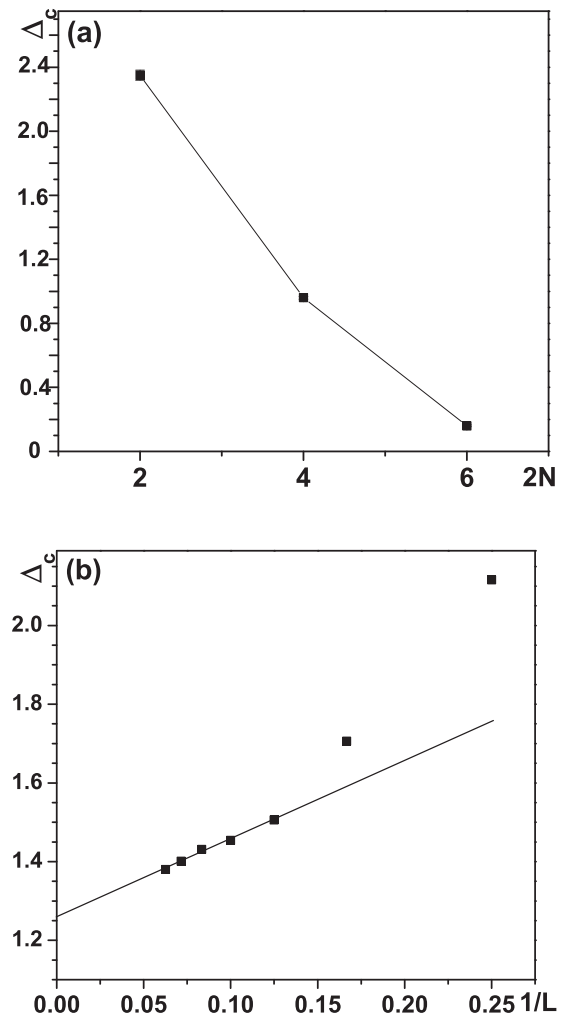

FIG. 4. Single-particle gaps of half-filled $SU(2N)$ Hubbard models. (a) Charge gaps with $U = 8$ at $2N = 2, 4$, and 6. (b) The $1/L$ scaling of the charge gap for the half-filled $SU(6)$ model at $U = 12$.

as the dimer order parameter. The structure factor of D_{ij} at $\vec{Q}' = (\pi, 0)$ and that of DDW at $\vec{Q} = (\pi, \pi)$, after being divided by L^2, and are plotted in Figs. 3(a) and 3(b), respectively. They are fitted by a power law $(1/L)^2$, thus their correlations are short ranged.

VI. SINGLE-PARTICLE GAPS

In this section, we further present the simulation results of the single-particle gaps for the $SU(4)$ and $SU(6)$ Hubbard cases.

The single-particle gaps are calculated at half filling through the onsite imaginary-time-displaced Green's function

$$G(0, \tau) = \frac{1}{L^2} \sum_i \langle \Psi_G | c(i, \tau) c^\dagger(i, 0) | \Psi_G \rangle, \quad (11)$$

where $|\Psi_G\rangle$ is the ground state. At long time displacement, $G(0, \tau) \rightarrow e^{-\Delta_c \tau}$ where Δ_c is the single-particle excitation gap, thus Δ_c can be fitted from the slope of $\ln G(0, \tau)$ vs τ. Let us consider the large-U limit for an intuitive picture: in the Mott-insulating background, the energy of adding a particle is lowered from U by further virtual particle-hole excitations. In other words, the Mott insulator is polarizable. As increasing $2N$, the configuration numbers of the virtual particle-hole excitations increase, which enhances charge fluctuations and thus reduces the single-particle gap. In Fig. 4(a), Δ_c's are plotted at a fixed $U = 8$ for $2N = 2, 4$ and 6, all of which are finite. For the $SU(6)$ case, $\Delta_c = 0.15$ is rather small at $U = 8$. Nevertheless, Δ_c increases to 1.26 at $U = 12$ at which the system is safely inside the Mott-insulating regime. The charge localization length can be estimated as $\xi_c \approx v_f / \Delta_c \approx 3 \sim 4$, which is much smaller than the maximal sample size $L = 16$.

VII. CONCLUSIONS

In summary, we have studied the ground-state quantum antiferromagnetism in a half-filled $SU(2N)$ Hubbard model in square lattice. For the case of $SU(4)$, a long-range AF order still survives with a much smaller value of Neel moment compared to that of $SU(2)$. For the $SU(6)$ case, we have found the absence of spin gap. The current numeric results are consistent with either a vanishing or very weak AF ordering beyond the resolution limit in this simulation. We have also found that the single-particle gap is strongly suppressed as N increases.

ACKNOWLEDGMENTS

APPENDIX A: METHOD OF THE PROJECTOR QUANTUM MONTE CARLO

At zero temperature, the ground-state (GS) wave function $|\Psi_G\rangle$ can be obtained by the projector quantum Monte Carlo
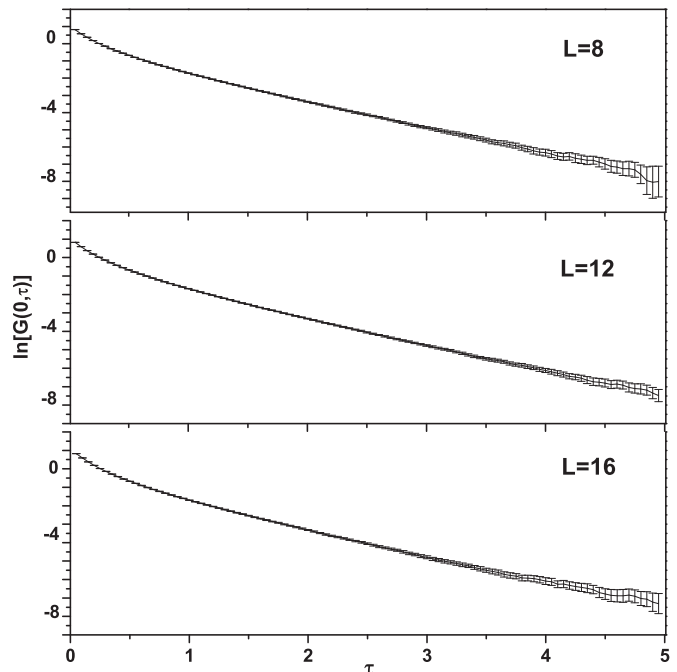

FIG. 5. The imaginary-time-displaced onsite Green's functions of the $SU(6)$ model for $U = 12$ with different sample sizes of $L = 8, 12$, and 16.

(PQMC) method, which projects a trial wave function $|\Psi_T\rangle$ in the following way:

$$|\Psi_G\rangle = \lim_{\beta \to \infty} e^{-\beta \hat{H}} |\Psi_T\rangle, \quad (A1)$$

where $|\Psi_T\rangle$ is required to be nonorthogonal to $|\Psi_0\rangle$. As β is large, these projection procedures can filter out states other than the GS. β plays the role as the projector parameter. The expectation value in the zero temperature limit is defined as:

$$\langle \hat{O} \rangle = \frac{\langle \Psi_0 | \hat{O} | \Psi_0 \rangle}{\langle \Psi_0 | \Psi_0 \rangle} = \frac{\langle \Psi_T | e^{-\frac{\beta}{2} \hat{H}} \hat{O} e^{-\frac{\beta}{2} \hat{H}} | \Psi_T \rangle}{\langle \Psi_T | e^{-\beta \hat{H}} | \Psi_T \rangle}. \quad (A2)$$

Similarly to the finite-temperature scheme, the zero-temperature problem can be formulated as the determinant QMC method with Suzuki-Trotter decompositions and auxiliary fields $\{l\}$, called projector quantum Monte Carlo (PQMC).

In the framework of the PQMC, the trial wave function is chosen as a ground state of the noninteracting Hamiltonian. We consider a free tight-binding Hamiltonian on the square lattice with a tiny magnetic flux Φ through the sample as

$$H_0 = -t \sum_{\langle ij \rangle} \left\{ c_j^\dagger c_i e^{i \frac{2\pi}{\Phi_0} \int_j^i d\mathbf{l} \cdot \mathbf{A}} + \text{H.c.} \right\}, \quad (A3)$$

where $\mathbf{A} = \Phi \mathbf{e_x} / L$ is the vector potential and $\Phi_0 = hc/e$. In Eq. (A3), we neglect the spin index for simplicity. The purpose of introducing the flux is to break the ground-state degeneracy at half filling for Eq. (A3). Due to the $SU(2N)$ symmetry, the trial wave function for all the $2N$ components can be chosen the same, and thus the total trial wave function is the direct product of them. In our simulations, we take $\Phi/\Phi_0 = 0.0001$.
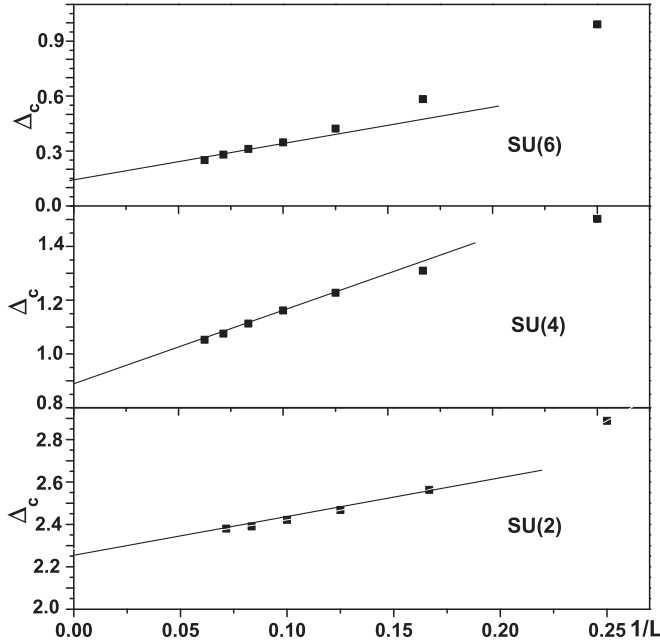
FIG. 6. Finite scalings of the single-particle gap for the half-filled $SU(2N)$ Hubbard model with $2N = 2, 4$, and 6 at $U = 8$. The extrapolated single-particle gap values are $\Delta_c = 2.26, 0.89$, and 0.15, for $2N = 2, 4$, and 6, respectively.

APPENDIX B: DERIVATIONS OF THE SINGLE-PARTICLE GAPS FROM THE TIME-DISPLACED GREEN's FUNCTIONS

We define the single-particle gap as the ground-state energy change of adding a particle to the ground state of the N-particle system as $\Delta_c = E_0(N+1) - E_0(N) - \mu$, where μ accounts for the changing of the particle number. The time-displaced Green's function is defined as

$$
\begin{aligned}
G^{>}(0,\tau) &= \langle \Psi_0^N | c_i(\tau) c_i^{\dagger} | \Psi_0^N \rangle \\
&= \frac{1}{L^2} \sum_i \langle \Psi_0^N | e^{\tau \hat{H}} c_i e^{-\tau \hat{H}} c_i^{\dagger} | \Psi_0^N \rangle \\
&= \frac{1}{L^2} \sum_{i,n} e^{-\tau(E_n^{N+1} - E_0^N - \mu)} \big| \langle \Psi_0^N | c_i | \Psi_n^{N+1} \rangle \big|^2. \quad \text{(B1)}
\end{aligned}
$$

Therefore, at large τ, we have $G^{>}(\vec{r} = 0, \tau) \sim e^{-\tau \Delta_c}$ to estimate the values of Δ_c.[39]

We present the QMC simulation results for the imaginary-time-displaced Green's functions for $U = 12$ in Fig. 5. The
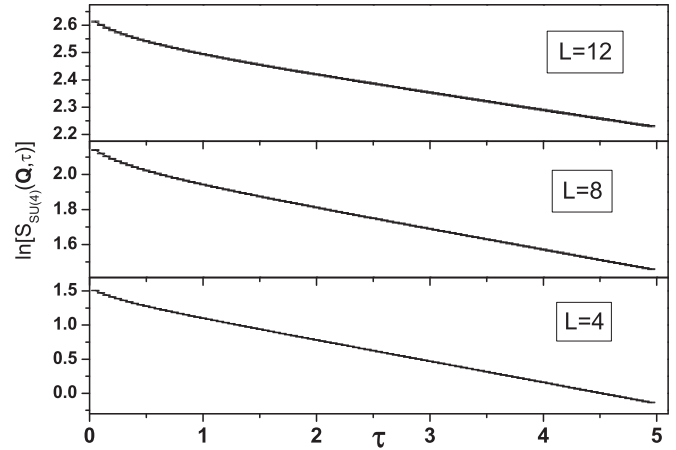

FIG. 7. The imaginary-time-displaced spin-spin correlation at momentum $\mathbf{Q} = (\pi, \pi)$ of the $SU(4)$ model for $U = 8$ with different sample sizes of $L = 4, 8$, and 12.

slopes of $\ln G(0, \tau)$ vs τ give rise the finite-size single-particle gap presented in Fig. 4(b) in the main text, in which the finite scaling shows that $\Delta_c = 1.26$. We also present the finite-size scaling of the single-particle gap values presented in Fig. 4(a) (main text) in Fig. 6. They are the single-particle gaps at $U = 8$ for half-filled $SU(2N)$ models with $2N = 2, 4$, and 6, which show the rapid decrease of gap values as increasing $2N$.

APPENDIX C: DERIVATIONS OF THE SPIN GAPS FROM THE TIME-DISPLACED SPIN-SPIN CORRELATIONS

The spin gap is defined as:

$$
\Delta_s(\vec{q}) = E_0(S = 1, N, \vec{q}) - E_0(S = 0, N), \quad \text{(C1)}
$$

in which $E_0(S = 1, N, \vec{q})$ denotes the ground-state energy with the total spin S, momentum $\vec{q}$, and particle number N. For the antiferromagnetic state, the spin gap $\Delta_s = \min_{\vec{q}} \Delta_s(\vec{q}) = \Delta_s(\vec{Q})$ with $\vec{Q} = (\pi, \pi)$.

To extract the spin gap, we define the imaginary-time-displaced spin-spin correlations at wave vector $\vec{Q}$ are defined as

$$
S_{SU(2N)}(\vec{Q}, \tau) = \sum_{\alpha\beta} \langle J^{\alpha\beta}(\vec{Q}, \tau) J^{\beta\alpha}(\vec{Q}, 0) \rangle. \quad \text{(C2)}
$$

Similarly to the derivation of the charge gap, we find that $S(\vec{Q}, \tau) \propto \exp[-\tau \Delta_s(\vec{Q})]$ as $\tau t \gg 1$. As shown in Fig. 7, the slopes of $\ln S(\vec{Q}, \tau)$ vs τ give rise the finite-size spin gap.

[1] J. E. Hirsch, Phys. Rev. B **31**, 4403 (1985).

[2] J. E. Hirsch, Phys. Rev. B **40**, 2354 (1989).

[3] D. P. Arovas and A. Auerbach, Phys. Rev. B **38**, 316 (1988).

[4] I. Affleck and J. B. Marston, Phys. Rev. B **37**, 3774 (1988).

[5] S. Sachdev and N. Read, Int. J. Mod. Phys. B **5**, 219 (1991).

[6] N. Read and S. Sachdev, Nucl. Phys. B **316**, 609 (1989).

[7] M. Hermele, T. Senthil, M. P. A. Fisher, P. A. Lee, N. Nagaosa, and X.-G. Wen, Phys. Rev. B **70**, 214437 (2004).

[8] P. W. Anderson and W. F. Brinkman, Phys. Rev. Lett. **30**, 1108 (1973).

[9] D. S. Rokhsar and S. A. Kivelson, Phys. Rev. Lett. **61**, 2376 (1988).

[10] R. Moessner and S. L. Sondhi, Phys. Rev. Lett. **86**, 1881 (2001).

[11] K. Harada, N. Kawashima, and M. Troyer, Phys. Rev. Lett. **90**, 117203 (2003).

[12] F. F. Assaad, Phys. Rev. B **71**, 075103 (2005).

[13] P. Corboz, M. Lajkó, A. M. Läuchli, K. Penc, and F. Mila, Phys. Rev. X **2**, 041013 (2012).

[14] J. B. M. A. Paramekanti, J. Phys. Cond. Matt. **19**, 125215 (2007).

[15] Z. Y. Meng, T. C. Lang, S. Wessel, F. F. Assaad, and A. Muramatsu, Nature (London) **464**, 847 (2010).

[16] C.-C. Chang and R. T. Scalettar, Phys. Rev. Lett. **109**, 026404 (2012).

[17] S. Yan, D. A. Huse, and S. R. White, Science **332**, 1173 (2011).

[18] H.-C. Jiang, H. Yao, and L. Balents, Phys. Rev. B **86**, 024424 (2012).

[19] N. Blümer and E. V. Gorelik, Phys. Rev. B **87**, 085115 (2013).

[20] P. Sinkovicz, A. Zamora, E. Szirmai, M. Lewenstein, and G. Szirmai, arXiv:1307.5726.

[21] R. K. Kaul and A. W. Sandvik, Phys. Rev. Lett. **108**, 137201 (2012).

[22] T. C. Lang, Z. Y. Meng, A. Muramatsu, S. Wessel, and F. F. Assaad, Phys Rev. Lett. **111**, 066401 (2013).

[23] S. Sorella, Y. Otsuka, and S. Yunoki, Sci. Rep. **2**, 992 (2012).

[24] S. Depenbrock, I. P. McCulloch, and U. Schollwöck, Phys. Rev. Lett. **109**, 067201 (2012).

[25] C. Wu, J. Hu, and S. Zhang, Int. J. Mod. Phys. B **24**, 311 (2010).

[26] C. Wu, J. P. Hu, and S. C. Zhang, Phys. Rev. Lett. **91**, 186402 (2003).

[27] C. Wu, Mod. Phys. Lett. B **20**, 1707 (2006).

[28] A. V. Gorshkov, M. Hermele, V. Gurarie, C. Xu, P. S. Julienne, J. Ye, P. Zoller, E. Demler, M. D. Lukin, and A. M. Rey, Nature Phys. **6**, 289 (2010).

[29] S. Taie, Y. Takasu, S. Sugawa, R. Yamazaki, T. Tsujimoto, R. Murakami, and Y. Takahashi, Phys. Rev. Lett. **105**, 190401 (2010).

[30] B. J. DeSalvo, M. Yan, P. G. Mickelson, Y. N. Martinez de Escobar, and T. C. Killian, Phys. Rev. Lett. **105**, 030402 (2010).

[31] S. Taie, R. Yamazaki, S. Sugawa, and Y. Takahashi, Nature Phys. **8**, 825 (2012).

[32] Z. Cai, H.-h. Hung, L. Wang, D. Zheng, and C. Wu, Phys. Rev. Lett. **110**, 220401 (2013).

[33] K. R. A. Hazzard, V. Gurarie, M. Hermele, and A. M. Rey, Phys. Rev. A **85**, 041604 (2012).

[34] L. Bonnes, K. R. A. Hazzard, S. R. Manmana, A. M. Rey, and S. Wessel, Phys. Rev. Lett. **109**, 205305 (2012).

[35] G. Sugiyama and S. Koonin, Ann. Phys. (N.Y.) **168**, 1 (1986).

[36] S. R. White, D. J. Scalapino, R. L. Sugar, E. Y. Loh, J. E. Gubernatis, and R. T. Scalettar, Phys. Rev. B **40**, 506 (1989).

[37] F. Assaad and H. Evertz, *Computational Many-Particle Physics*, Lecture Notes Phys. 739, (Springer, Berlin, 2008).

[38] F. F. Assaad, arXiv:cond-mat/9806307.

[39] F. F. Assaad and M. Imada, J. Phys. Soc. Jpn **65**, 189 (1996).

[40] M. Feldbacher and F. F. Assaad, Phys. Rev. B **63**, 073105 (2001).